




## Article

# The Effect of Anodization and Thermal Treatment on Mixed-Oxide Layer Formation on Ti–Zr Alloy

Ioana-Alina Ciobotaru <sup>1</sup>, Fidan Bahtiar Ismail <sup>2</sup>, Roxana Budei <sup>2,3</sup>, Anca Cojocaru <sup>1</sup>  
and Danut-Ionel Vaireanu <sup>1,4,5,\*</sup>

<sup>1</sup> Faculty of Chemical Engineering and Biotechnology, National University of Science and Technology, 011061 Bucharest, Romania; ioanaalinaciobotaru@yahoo.com (I.-A.C.); anca.cojocaru@chimie.upb.ro (A.C.)

<sup>2</sup> Faculty of Dentistry, University of Medicine and Pharmacy Carol Davila Buchares, 020021 Bucharest, Romania; fidan.ismail@umfcd.ro (F.B.I.); roxana-eliss.budei@umfcd.ro (R.B.)

<sup>3</sup> Dentix Millennium SRL, 087153 Sabareni, Romania

<sup>4</sup> Technical Sciences Academy of Romania, 030167 Bucharest, Romania

<sup>5</sup> Academy of Romanian Scientists, 050044 Bucharest, Romania

\* Correspondence: di\_vaireanu@yahoo.co.uk

**Abstract:** The anodization or thermal treatments applied to alloys of titanium and zirconium have a substantiated effect on the mixed-oxide layer formation compared to the naturally occurring one. A Ti–Zr 50%/50% alloy was chosen for a comparative study. Controlled, thermally treated, and anodized samples obtained with controlled procedures were analyzed in terms of morphological and compositional analysis (using SEM and EDX analysis) as well as for the determination of hardness variations. Substantial differences were observed depending on the applied functionalization method (compact of structured mixed-oxide nanotubes when the samples are subjected to the anodization procedure); there was an increase of more than six folds in the mixed-oxide layer hardness and D Shore scale, when subjected to thermal treatment, and hence, this lead to the conclusion that one may control the morphology, composition and/or the hardness of the mixed-oxide layer by applying one or another or a combination of functionalization methods.

**Keywords:** anodization; thermal treatment; Ti–Zr alloy; mixed-oxide



**Citation:** Ciobotaru, I.-A.; Ismail, F.B.; Budei, R.; Cojocaru, A.; Vaireanu, D.-I. The Effect of Anodization and Thermal Treatment on Mixed-Oxide Layer Formation on Ti–Zr Alloy. *Coatings* **2024**, *14*, 1217. <https://doi.org/10.3390/coatings14091217>

Academic Editors: Lei Guo and Cecilia Bartuli

Received: 15 August 2024

Revised: 19 September 2024

Accepted: 19 September 2024

Published: 20 September 2024



**Copyright:** © 2024 by the authors. Licensee MDPI, Basel, Switzerland. This article is an open access article distributed under the terms and conditions of the Creative Commons Attribution (CC BY) license (<https://creativecommons.org/licenses/by/4.0/>).

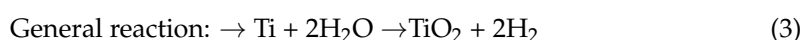
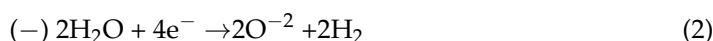
## 1. Introduction

The use of Ti–Zr alloys instead of pure titanium is becoming increasingly attractive for medical devices due to the inherent synergistic advantages of the two metals compared to each pure metal alone [1–4]. Abutments with a zirconia surface, in addition to excellent aesthetic properties, also have outstanding biocompatibility and good mechanical properties. Although both titanium and zirconium oxides are considered bioinert, problems associated with peri-implant soft tissues that lack hemidesmosome structures, vertical collagen fibers, and effective blood supply pose challenges for improving gingival adhesion to abutments [5]. Electrochemical treatments such as electrochemical anodization or electrochemical deposition can lead to obtaining a composite or nanostructured coating on titanium and zirconium surfaces and can significantly improve osseointegration and antibacterial properties [6,7]. Farrag et al. conducted a clinical study detailed in their article, which investigated the impact of anodized titanium on the health and appearance of peri-implant soft tissue. In this context, anodic oxidation serves as a surface modification method aimed at altering the color of titanium abutments. Titanium naturally forms an oxide layer on its surface immediately upon contact with atmospheric air. The process of anodic oxidation enhances the thickness of this oxide layer, which is influenced by the voltage applied during oxidation. By manipulating the thickness of the oxide layer, distinct colors can be achieved as it interacts with light in various ways [8].

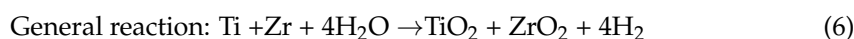
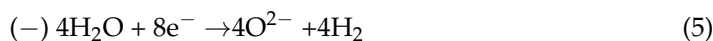
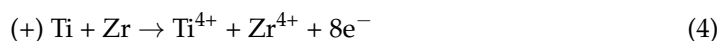
The anodizing process involves the application of an anodic potential to the surface of a metal, specifically pure titanium or a Ti–Zr 50%/50% alloy, to either dissolve the anode or generate dense oxide films on its surface. This oxide layer forms through ion migration, where ions move in alignment with the electric field. Metal cations are released from the bulk of the metal, while oxygen anions are sourced from the electrolyte, traversing through lattice imperfections, vacancies (both anionic and cationic), and interstitial defects. In the case of titanium and zirconium, the growth rate of the oxide layer is limited by the migration of  $O^{2-}$  ions from the film/electrolyte interface to the metal/oxide interface, where the  $O^{2-}$  ions react with oxidized titanium or zirconium,  $Ti^{4+}/Zr^{4+}$  [9,10].

The reactions that occur are as follows:

For pure titanium:



For the Ti–Zr 50%/50% alloy (the anodic potential is high enough to allow simultaneous oxidation of Ti and Zr):



The thickness of the oxide film is directly dependent on the total electric charge in the system, the anodization time, and the density of the oxides. The thickness of the oxide layer is influenced by the overall electric charge within the system, the duration of anodization, and the oxide density. Pauporté et al. investigated the anodic formation of titanium and zirconium oxide films in a NaOH environment using electrochemical impedance spectroscopy and scanning electron microscopy. Their research revealed a strong correlation between the thickness measurements obtained through the EIS technique and direct observations of the films cross-section. This led to the hypothesis that the outer layer of the oxide film contains very small pores, allowing the electrolytic solution to penetrate into the defects of the film [11]. There is a dispute regarding the crystalline and amorphous nature of the titanium dioxide and zirconium produced on the surface of the metal layer.

Researchers have indicated that the amorphous structure changes to a crystalline form at temperatures between 400 and 600 °C. The temperature at which titanium dioxide or zirconia is transformed from the amorphous phase starts around 300 °C, and the transition is gradual [12]. It was shown that the anatase (101) crystal plane appears first, and the other crystal planes appear in order. The rutile (110) crystal plane appears first, and the other crystal planes appear in successive order, thus the rutile (110) crystal plane has the lowest energy and is the most stable, so it is not recommended to exceed a temperature of 500 °C for this transition, as the subsequent crystalline forms are gradually less stable [12–14].

Liu et al. used the electrochemical anodization technique to improve zirconia surfaces by removing oxygen from solid metal oxides via molten salt electrolysis. They suggested that the anodized zirconia exhibits well-ordered and low microporous contact angles and a slight decrease in monoclinic phase content [15]. The nanotube structure is characterized by easy control of pore size, large surface area, chemical stability, mechanical stiffness and excellent compatibility [16,17]. Tsuchiya et al. showed that electrochemical anodization could form highly organized zirconia nanotubes with diameters of about 50 nm–130 nm and a length of 17  $\mu\text{m}$  [18]. Guo et al. showed that when zirconia nanotubes were immersed in simulated body fluids for 20–30 days, bone-like apatite could form on the surface of zirconia nanotubes, indicating that zirconia nanotubes could exhibit favorable bioactivity [19]. Jennes et al. conducted a study in which they systematically reviewed articles dealing with

antibacterial surfaces or coatings of implant abutments that can suppress bacterial growth and thus prevent plaque-induced peri-implant inflammatory diseases [20].

The reviewed literature shows that electrochemical treatments such as anodization, electrochemical deposition or any other combined functionalization that include anodization of Zr-containing Ti alloys which lead to an increased corrosion resistance besides improved mechanical properties, have enhanced biocompatibility and a favorable price–performance ratio. These treatments produce a composite or a nanostructured coating on titanium surfaces that can significantly improve adhesion and antibacterial properties [6,21–25]. After comparing the literature data for the most commonly used types of treatment for impact surfaces, it can be stated that (a) the roughness created on the metal surface is determined by the size, shape and velocity of the particles used in the sandblasting process, while in electrochemical anodizing, the nanotube structure is characterized by an easily controllable pore size, large surface area, chemical stability, mechanical strength and excellent compatibility; (b) compared to anodizing, which can be applied to conductive materials, the sandblasting process can also be applied to non-conductive materials such as ceramics or cermets (metallized ceramics), but the results produce anisotropic abrasion with unevenly distributed roughness.

The main disadvantage of the sandblasting technique is that it can slightly change the chemical nature of the surface due to the inevitable contamination by aluminum oxide, whereas with electrochemical anodizing, the surface contamination can come from traces of the remaining electrolytic solution. (c) Unlike blasting and anodizing surface treatments, plasma treatment can remove low-energy surface contaminants, clean and increase surface free energy and improve cell adhesion kinetics. (d) Compared to sandblasting and acid etching techniques, laser treatment carries zero risk of surface contamination, as there is no direct contact between the laser and the biomaterial.

Laser surface treatments, sandblasting and acid etching enhance the wettability of materials by altering their surface characteristics, which are crucial for promoting cell adhesion.

The purpose of this work was to investigate the influence of the anodization and thermal treatment applied to a Ti–Zr alloy on the morphology and composition of the mixed-oxide layer formed at the surface of this alloy and on the hardness of the oxide layer subjected to thermal treatment compared to the untreated ones. This study holds considerable significance as it offers a comparative analysis of distinct and combined functionalization techniques, specifically anodization and thermal treatment, applied to a Ti–Zr alloy. It aims to produce oxide layers with improved characteristics, which could be beneficial for applications in corrosion protection and restorative dentistry.

## 2. Materials and Methods

The chemical reagents used were of *p.a.* and were from Sigma-Aldrich/Merk, (Merck KGaA, Darmstadt, Germany). The solutions, where the case is, were prepared using ultra-pure water that have the value of resistivity  $>18.5 \text{ m}\Omega\cdot\text{cm}$ . The Ti–Zr alloy rods (50% Ti–50% Zr) CSTY202116 (ZrTi-50  $\pm$  2%, Fe 0.2%, Si 0.5%, Vickers Hardness 300) were purchased from Baoji City Changtai Metals Trading Co., Ltd., Xiamen, China) and were cut in disks with a diameter of 32 mm and thickness of 1.2 mm using a Citizen Cincom (Esslingen, Germany) L20 8M CNC computer-controlled lathe with 6 linear axes and two rotary axes. The chosen composition of 50% titanium and 50% zirconium was selected for its ability to merge the advantageous characteristics of both metals, including biocompatibility, strength, corrosion resistance, osseointegration, and gum adhesion. This formulation also mitigates the predominant influences of either metal during the analytical phase.

The disks were wet polished with 200, 600, 2000 and 4000 Optimus Colad emery paper with sponge support to prevent damaging the surface, followed by a finer finish polish with diamond paste (see Supplementary Materials Figure S1), and then washed thoroughly and rinsed with distilled water. The disks were immersed in an ultrasonic bath (@40 kHz) containing distilled water with 0.1% liquid detergent for advanced cleaning, for 10 min,

rinsed with ultrapure water, dried, immersed in isopropyl alcohol 96%, dried by blowing with air at a pressure of 1.5 bar and subjected to the following treatments:

- Sample with index 1—blank sample, control, mixed-oxide layer formed naturally;
- Sample with index 2—non-anodized sample, thermally treated at 450 °C;
- Sample with index 3—anodized and thermally untreated sample;
- Sample with index 4—sample anodized and heat treated at 450 °C.

A furnace made with a thermostated electrical double-insulated refractory cylindrical longitudinal furnace (300 mm external diameter and 500 mm total length) was used for thermal treatment. Its core was a hollow cylinder on the inside with an internal diameter of 60 mm, provided with a K-type thermocouple temperature probe (−50 °C~1300 °C). The cylindrical, longitudinal ceramic element is wrapped in a high-power electrical resistance material connected to a variable voltage a.c. power supply with the possibility of varying the voltage applied to the resistor terminals at will. Adjusting the applied voltage directly influences the current passing through the resistor, allowing for precise control of the temperature within the ceramic tube. To enhance energy efficiency, the space between the active component and the outer cylinder is filled with refractory chamotte, which serves to insulate and direct the heat produced by the resistor towards the inner ceramic cylinder. By managing the applied voltage, the furnace can maintain a wide range of regulated temperatures from 60 to 600 °C over prolonged durations.

The furnace was calibrated prior to use (basically, the applied voltage was set to the desired value and the temperature in the furnace was recorded after 15 min using the temperature probe and the digital thermometer connected to the temperature probe). The furnace was brought to the desired temperature before each experiment and kept there for 15 min to achieve thermal equilibrium before the sample was inserted. A blank control sample with the mixed-oxide layer formed naturally was also initially tested to see whether it was a compact one and whether it offers a certain degree of protection against corrosion attacks. To achieve this, two well-established electrochemical techniques were used: open circuit potential, OCP, and electrochemical impedance spectroscopy, EIS. OCP measurements are also required as a preliminary conditioning stage for EIS measurements.

OCP is also known as open circuit voltage, zero current potential, corrosion potential, equilibrium potential, or resting potential. This measurement is a fundamental electrochemical technique used to assess the susceptibility and development of a reaction in a specific corrosion environment. In measuring open circuit potential, the test material is placed in an electrolyte in conjunction with a stable, non-polarizable reference electrode and the evolution of the material's potential relative to the reference electrode is monitored. This is also called corrosion potential monitoring. The reference electrode is a non-polarizable one with a very high internal resistance, e.g., gigaohms, so that the value of the current passing through the circuit made of the two electrodes is practically zero. In this way the potential difference between the two electrodes can be considered as an electromotive voltage.

If the value of the potential increases over time, progressing towards more electronegative values, this indicates an increase in the protective capacity of the passivation layer on the metal surface, indicating greater corrosion resistance. On the other hand, when the potential values tend to go toward more electropositive values, this may indicate a greater susceptibility to the reaction in the chosen electrolyte. Electrochemical impedance spectroscopy is a non-destructive electrochemical analysis method that provides information about the electrochemical properties of the tested systems. This technique measures the impedance, i.e., resistance to alternating current, at the interface of the electrochemical system. One of the important parameters measured in EIS is the charge transfer resistance, which indicates the degree of difficulty in the transfer of charges from the electrode to the surface of the electrochemical interface.

In EIS, impedance is measured as a function of frequency and is plotted as a Nyquist plot or Bode plot. The analysis of these diagrams can provide detailed information about the electrochemical processes taking place at the interface of the analyzed system such as charge transfer resistance, electric double layer capacity etc. Charge transfer resistance ( $R_{ct}$ )

is one of the important parameters in EIS. This is defined as the resistance to the transfer of charges from the electrode surface to the electrochemical interface and is influenced by the properties of the electrochemical interface, the structure and composition of the medium, as well as the properties of the deposited oxide layer, essentially its thickness. Being a directly measurable quantity, the assessment will be quantitative.  $R_{ct}$  can be obtained from the Nyquist plot, which is a graphical representation of measured impedance versus frequency.

Impedance is usually measured by applying an alternating potential to the electrochemical cell and measuring the current in the cell. When a sinusoidal potential is applied, the response is an alternating current signal containing the frequency and shape of the signal. The current signal can be analyzed as a sum of sinusoidal functions. Electrochemical impedance is usually measured with a small excitation signal, so the cell response is pseudolinear. The equipment used for the above experimental determinations was a computer controlled Voltalab 40 potentiostat/galvanostat, equipped with EIS module and digital data acquisition system, where the recordings of the potential data in the open circuit, as well as electrochemical impedance spectra, were carried out. For EIS, a potential disturbance of 10 mV above the given voltage value of OCP in the frequency range of 100 kHz–100 mHz was used. The full experimental protocol, as well as the complete depiction of all operational parameters is found in the Supplementary Materials Figure S2–S6, integrated part of this paper.

The electrochemical tests described above were carried out in a three-electrode electrochemical cell made of PTFE (a glass cell is not suitable as the fluoride ions from the electrolyte attack the glass and this leads to a decrease in the available fluoride ion concentration); the working electrode was a Ti–Zr alloy disk (active immersed surface of 25.26 cm<sup>2</sup>); a saturated silver/silver chloride reference electrode was used (Radiometer Analytical), fitted with a Luggin capillary; a mesh platinum electrode was used as the auxiliary electrode; and the electrolyte was the anodizing solution presented in Table 1. To avoid accidental cross-contamination, the disks were held by a Ti medical Grade 4 rod with a slit at the holding points slightly smaller than the disk thickness, so that the disk is held in place by pressure and friction (see Supplementary Materials Figures S2–S6).

**Table 1.** The chemical composition of the electrolyte used for anodization and electrochemical tests.

Constitutive Component	Mass %
Ethylene glycol (ethane-1,2-diol)	96.10
Oxalic acid (C <sub>2</sub> O <sub>4</sub> H <sub>2</sub> )	0.2776
Water (H <sub>2</sub> O)	3.30
Ammonium fluoride (NH <sub>4</sub> F)	2.4·10 <sup>−3</sup>
Choline chloride (C <sub>5</sub> H <sub>14</sub> ClNO)	0.32

The anodization and the thermal treatment procedures.

A number of four Ti–Zr alloy samples (50%/50%, mass percentages), coded as above, were considered for testing the combined anodization/oxide thermal conversion effect. A ceramic support was used to allow for an easy introduction of the samples in the furnace, as shown in Figures 1 and 2. The anodization was carried out in a PTFE beaker (to prevent the loss of fluoride) employing a two-electrode cell, in a mixed potentiostatic and galvanostatic setup, using a constant current–constant voltage power supply SPS-12003N ( $U_{max} = 120$  V,  $I_{max} = 3$  A) provided with precision digital ammeter, voltmeter and wattmeter. If the anodization is performed at voltages above 30 V, then the conversion of the amorphous phase into the crystalline phase of Ti and Zr oxides is performed at temperatures between 400 and 500 °C.

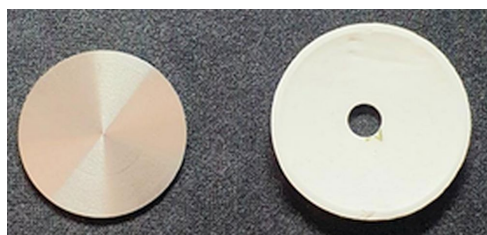


**Figure 1.** A blank sample and the ceramic support.



**Figure 2.** A blank sample put on the ceramic support ready for the thermal treatment.

The following anodizing stages and the thermal conversion were chosen for this procedure:

1. Determination of the working current density: the sample is pre-anodized at a constant voltage of 35 V for 180 s. At the end of the period, the value of the current is read.
2. The configuration of the anodizing electrical source is changed from potentiostatic to galvanostatic, and the value of the anodizing current is kept constant and equal to the value determined in the pre-anodization stage. Knowing the required current density and measuring the surface area of the sample allows for straightforward calculation of the anodization current. The anodization process is performed in galvanostatic mode, maintaining a constant current to ensure that the electrochemical reaction rate remains stable, as the current density directly influences this rate during the anodization.
3. The sample is anodized for a period of 30 min, following the variation of the anodizing voltage over time.
4. The thermal conversion was carried out for a period of 15 min, in the presence of excess air supplied by introducing an air flow of 5 L/min, (see Supplementary Materials Table S1 for the flow rate calibration) timed from the point when the furnace reached the temperature of 450 °C, and this temperature was kept constant by the thermostating device.

SEM/EDX analysis was performed using an Apreto S microscope (Thermo Fisher Scientific, Waltham, MA, USA) equipped with an EDAX Inc., Mahwah, NJ, USA, device. The SEM micrographs were recorded applying an accelerating voltage of 10 kV and a current of 6.3 pA, standard ETD, scale 20–400  $\mu\text{m}$ , magnification  $70\times$ – $40,000\times$ , while the elemental composition was determined based on the data recorded using the TEAMTM software V1.10. (15 kV and 1.6 nA).

For the comparative evaluation of the hardness of mixed oxides obtained by anodization versus anodization and thermal treatment, we used the Shore scale employing a modified Shore hardness tester. The Shore hardness is rated on the International RHardness Degree scale normalized in centigrade, from 0 to 100. The higher the number indicated, the harder the material will be. Values between different Shore classes can be made equivalent to each other or to other scales (e.g., Rockwell or Brinell) using either tables, equivalence charts or regression equations (see Supplementary Materials Figures S7–S11 and Table S3). A modified certified Hardness Shore D digital tester type 560-10D (certification number 0021787/2024 certified for ISO 868/2003 stan [26]) supplied by Heli Innovation Ltd., Sofia, Bulgaria with a penetration force of 44.5 N and a 0.5 D resolution was used to assess the differences in hardness of the obtained mixed oxides between anodized disks and anodized



and thermally treated disks. This was mounted on a specially constructed stand to ensure a reproducible perpendicular position, and the conical probe was replaced with a tronconical one. A correction factor  $K$  was determined to take into consideration the shape of the tronconical probe versus the conical one. The measurements were carried out in series of 5 replicated tests.

### 3. Results and Discussions

#### 3.1. Preliminary Electrochemical Tests—OCP and EIS Measurements

The results obtained from the preliminary electrochemical tests are presented in Figures 3 and 4.

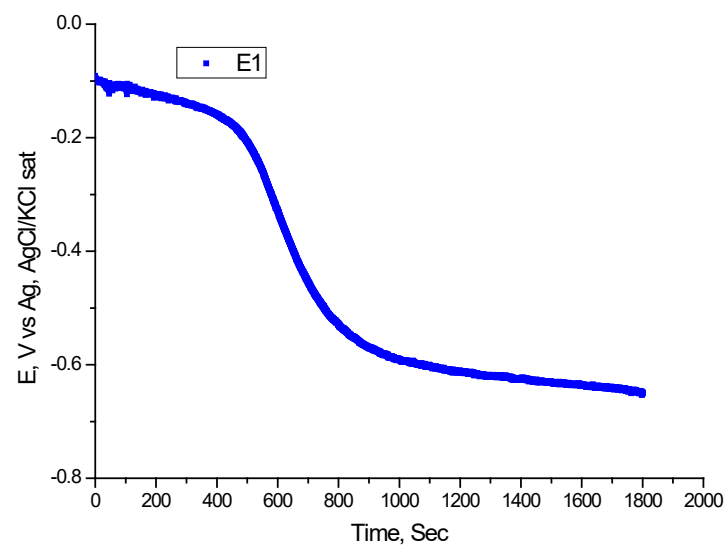


**Figure 3.** The variation of the open circuit potential with time (E1-electrolyte 1, see Table 1).

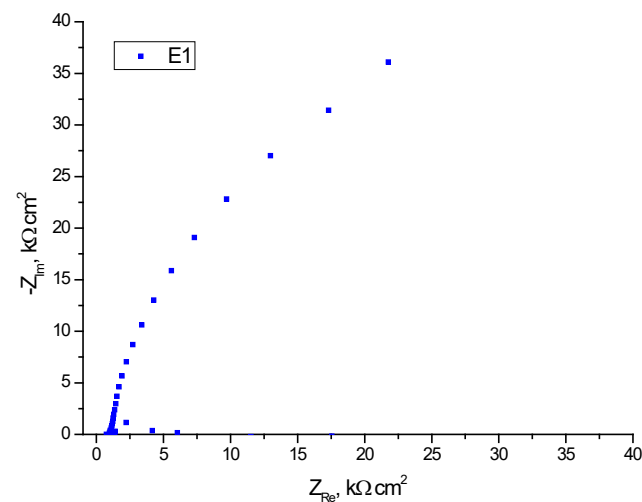


**Figure 4.** The Nyquist diagram registered for the studied electrolyte.

From the OCP graphical representation, as shown in Figure 3, one may see that the values of the relative potential evolve towards more negative ones and there is a tendency for stabilization, indicating a low susceptibility to corrosion and the existence of a stable mixed-oxide layer, even in the presence of fluoride ions. Therefore, should one need to increase the thickness of the mixed-oxide layer formed naturally, an anodization procedure may be employed successfully. This is also confirmed by the EIS measurements, see Figure 4, and the data represented in Figure 4 are of paramount importance as they supply

the necessary information in terms of real impedance and imaginary impedance to be processed in order to model the equivalent circuit. The capacitive semicircle observed is directly related to the oxide film formed on the surface and the value of the polarization resistance obtained from this graph is directly related to the thickness of the oxide layer formed.

### 3.2. Anodization and Thermal Treatment

The results obtained for the calibration of the electrical furnace and the correspondent regression equation are presented in Figure 5.

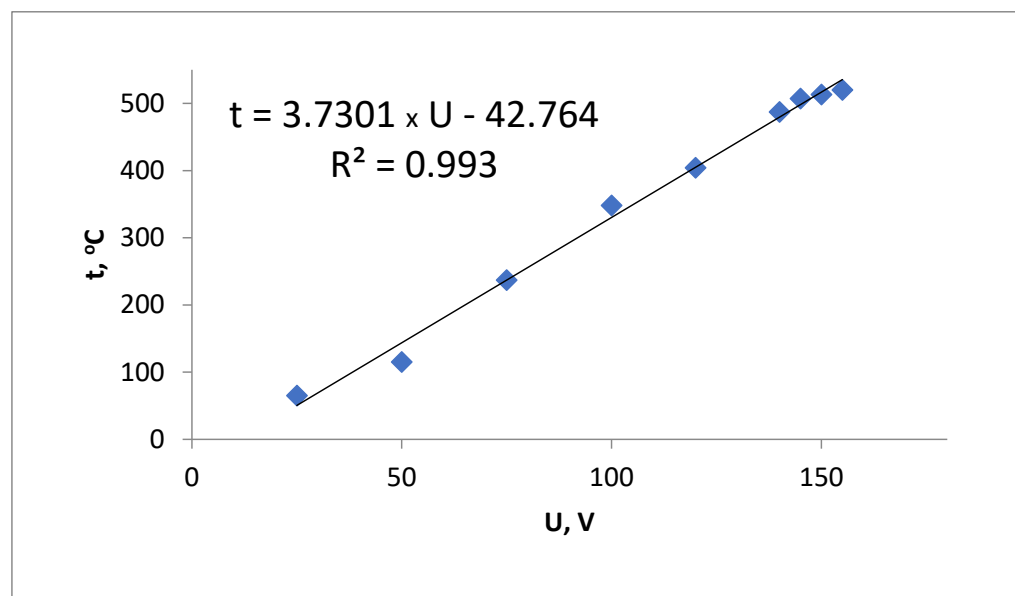


**Figure 5.** Electrical furnace calibration graphical representation ( $t$ , temperature, °C;  $U$ , applied a.c. voltage, V; and  $R$ , correlation coefficient).

The advantage of using an electrical furnace is that by carefully controlling the applied voltage, one may obtain the desired working temperature for the thermal treatment. In order to have full control, the furnace was initially calibrated (see Figure 5). By applying a step-by-step increase in voltage, one measures the inner core temperature of the furnace after it reaches the thermostated regime. The results obtained for the calibration of the electrical furnace are presented in Figure 5. A correspondent regression equation for the acquired data was calculated and is presented Equation (7). This transfer function allows the setting of the desired temperature with variations of  $\pm 5$  °C (induced by the thermostatic system) by changing the applied electrical voltage.

$$t = 3.730 \times U - 42.764 \quad (7)$$

where  $U$  is the applied voltage, V and  $t$  is the temperature in °C

As far as the anodization process driven in galvanostatic mode is concerned, once the value of the working current density and implicitly of the electric current intensity was obtained (see the anodizing procedure), this it kept constant throughout the anodizing process, to maintain the speed of the electrochemical process at a constant value and ensure a uniform growth rate for the titanium and zirconium oxides, and the voltage variation in time was monitored. The anodizing voltage values versus time are shown in Figure 6 and a depiction of photographed samples is presented in Figure 7. The anodizing voltage values versus time represented in Figure 6 shows a curve shape typical for constant current density operation, namely a high value at the beginning of the process, indicating the maximum equivalent ohmic drop in the electrolyte solution, followed by a decrease in time of the registered voltage. This decrease in the anodizing voltage value over time can be



explained by the release of an increased number of titanium and zirconium ions by the attack of fluoride ions, and, as time goes by, this leads to an increase in the conductivity of the electrolyte solution.

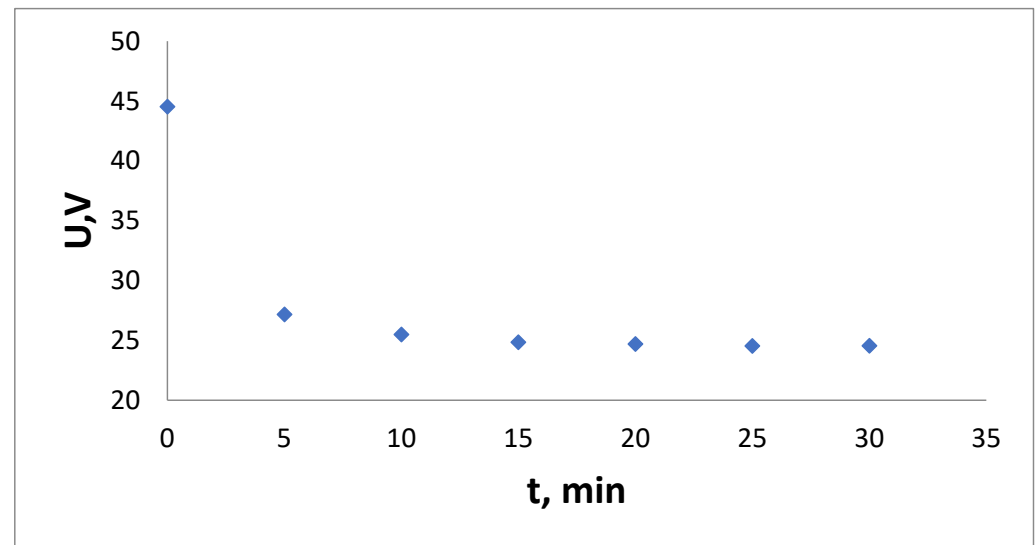


**Figure 6.** The variation of the anodizing voltage versus time in galvanostatic mode, at  $i = 2.52 \text{ mA/cm}^2$ ,  $t = 30 \text{ min}$ .

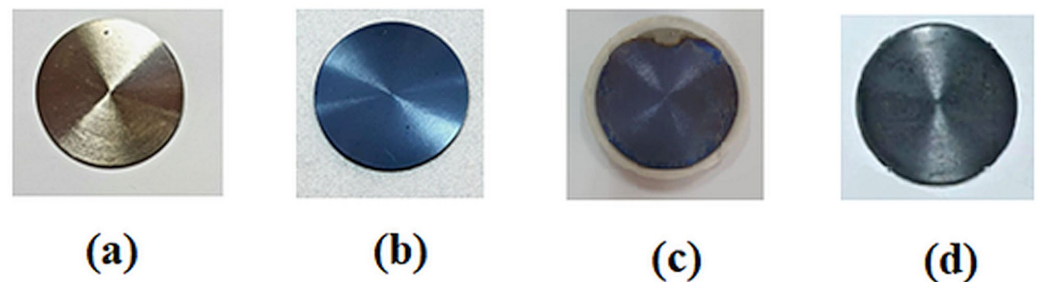


**Figure 7.** Photographs of blank and functionalized samples. (a) DAT1, blank sample; (b) DAT2, thermally treated sample; (c) DAT3, anodized sample, prepared for thermal treatment; and (d) DAT4, anodized and thermally treated sample.

As the procedure is set to work in galvanostatic conditions, the higher the electrolyte conductivity, the lower the ohmic drop, and hence the electronic power supply regulatory system will act to maintain the current constant by decreasing the applied voltage. In Figure 7, one may clearly see the differences occurring when one uses various functionalization methods. Figure 7a represents the blank sample, naturally occurring oxide. As the sample is thermally treated, the color changes, indicating the formation of new oxide layers on top of the naturally occurring ones. The color changes as well for the layers of oxide formed by anodization, Figure 7c, and dual treatment, anodization and thermal treatment, Figure 7d, indicating a change in the layer morphology as well as layer thickness. The anodizing voltage values and their variation in time fit very well in the anodizing voltage range reported in the literature for similar anodizing conditions and in similar electrolytes [21–23].

### 3.3. SEM Analysis

The surface of the studied samples was scanned with an electron beam targeting the sample surfaces, with the result being an emission of secondary electrons and X-rays specific to the component elements. The anodized and thermally treated samples were

subjected to morphological and compositional investigations. The comparative results are presented in Figure 8.

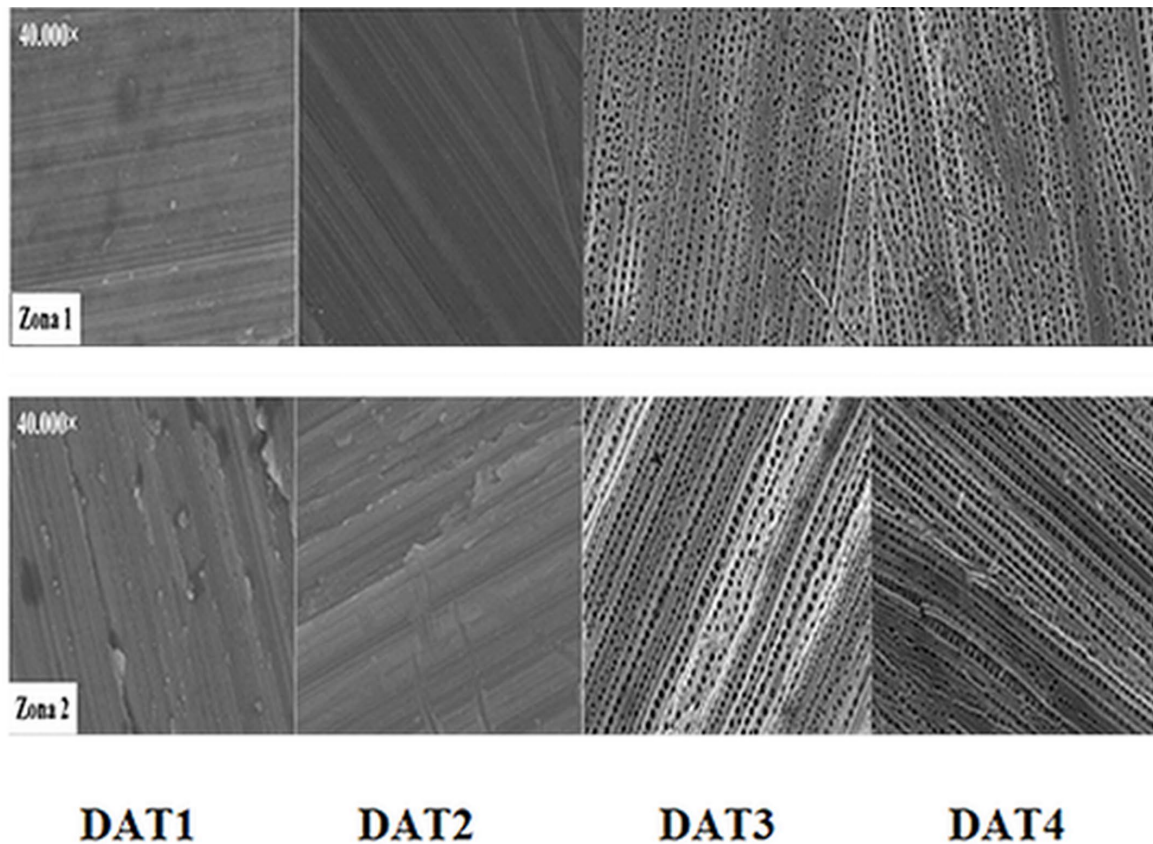


**Figure 8.** Comparative SEM micrographs of the investigated samples (where DAT1, blank sample; DAT2, thermally treated sample; DAT3, anodized sample, thermally untreated; and DAT4, anodized and thermally treated sample).

SEM analysis, Figure 8, reveals that the desired layers of titanium and zirconium oxides are obtained, clearly outlined, and well-formed. A fact worth noting is the thermal effect from the heat treatment, which managed to remove most of the contamination with organic carbon which is converted at the working temperature in the form of  $\text{CO}_2$  and water and is eliminated by driving with the flow of pressurized air. This pressurized inflow of air provides the necessary excess oxygen, in a continuous flow, to oxidize the areas that have small crevasses/cracks from the anodization and, at the same time, converts the amorphous form of the oxides into a crystalline form that are much harder, more adherent and more resistant to mechanical abrasion compared to the amorphous form. This thermal treatment, performed after anodization, with a synergistic effect leads to an improvement in the oxide layers formed.

The control sample (DAT1) exhibits, over its entire surface, a compact layer, with visible structural defects characteristic for the natural state of this alloy. In sample 2, DAT2, the disk is subjected to a heat treatment at  $450\text{ }^\circ\text{C}$  in air for 15 min, and it exhibits the same morphology as the control sample, but in addition, it clearly shows the formation of a more compact mixed oxide  $\text{TiO}_2\text{-ZrO}_2$ , which is thermally induced in an excess of oxygen leading to a decrease in the number of defects as a result of the composition analysis (Figure 9). In contrast, the anodized sample DAT3, exhibits homogeneous surface properties and the presence of porous nanostructures can also be observed.

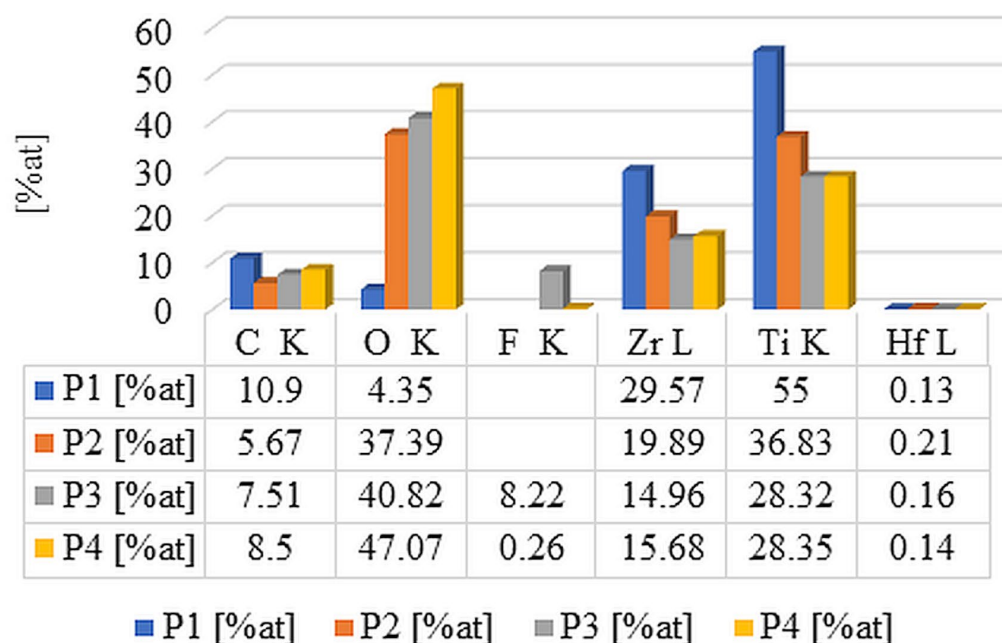


**Figure 9.** Comparative compositional analysis of treated and untreated samples calculated as average of three investigated zones for each sample (P1 = DAT1, P2 = DAT2, P3 = DAT3, and P4 = DAT4).

These structures are highly desirable in the functionalization of these materials and are specific for anodization processes in fluorinated electrolytes when oxide nanotubes are formed from the metal substrate material. They have potential applications in restorative dentistry by improving the process of osseointegration and the adhesion of gingival cells to these functional materials. Sample DAT4, Figure 8, (anodized and heat-treated disc) also exhibits very similar structures to sample DAT3 over the entire analyzed surface. The question that remains to be answered, and will be answered below, is whether or not post-anodization heat treatments modify the hardness of the mixed oxide layer. EDX measurements were performed in three distinct areas at 3000 $\times$  magnifications. The results of the compositional analysis are comparatively summarized in Figure 9 and presented in extenso in the Supplementary Materials Figures S12–S15 and Tables S4–S7. Although EDX analysis is not appropriate for quantitative quantification of C and O content, the information was presented to see whether or not there is a variation in their content and to see if any modifications may occur depending on the functionalization method.

### 3.4. Shore D Hardness

The results of Shore D hardness registered for the analyzed samples are presented in Table 2.

As one may see from Table 2, the Shore D hardness values of a series of five replicated samples are well grouped for both functionalization methods, namely anodization as well as anodization followed by thermal treatment. The thermal treatment appears to play an important role in increasing the Shore D hardness by six folds, a beneficial effect for enhancing the mechanical properties of the deposited mixed oxide layer (the correction factor K was used when calculating the corrected average values to take into consideration the shape of the tronconical probe versus the conical ones).

Data obtained from the preliminary electrochemical tests were beneficial in constructing a model that supplies quantitative parameters related to the metal/oxide interface. This is particularly important as the pores or defects in the oxide structure will distort the semicircle shape of the Nyquist representation and may offer a very good indication regarding the homogeneity and lack of defects of the formed mixed-oxide layer. The model proposed was constructed using a dedicated software, Zview 2.70 (Scribner Associates,

Inc., New York, NY, USA), and the outcome of this model is presented in Figure 10 and in Table 3.

**Table 2.** Comparative values of Shore D hardness for surfaces functionalized by anodization and anodization followed by thermal treatment (where A. is anodization and A.+T.T. is anodization and thermal treatment); the values are dimensionless.

Sample	Shore D	Average	Standard Deviation	K	Shore D, Corrected
1	2.5				
2	2.5				
3	2.0	2.4	0.22		2.7
4	2.5				
5	2.5				
6	14.0			1.125	
7	15.5				
8	14.5	14.7	0.57		16.5
9	14.5				
10	15				

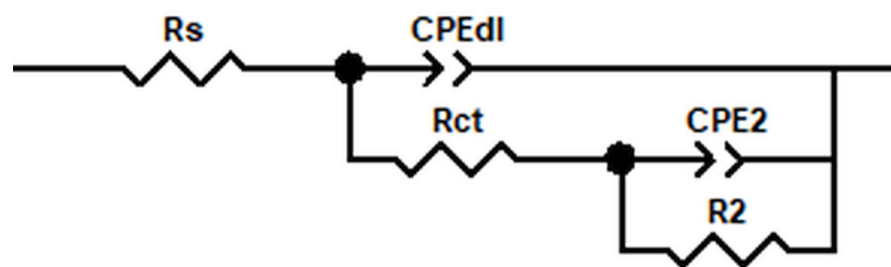


**Figure 10.** The model of the equivalent circuit.

**Table 3.** The characteristic parameters obtained from EIS measurement and their equivalence with the model parameters.

EIS Data from Equivalent Circuit	E1
$R_s$ (Ohm·cm <sup>2</sup> )	1.911
$CPE_{dl}$ (F·cm <sup>-2</sup> )	0.625
$R_{ct}$ (kOhm·cm <sup>2</sup> )	2.867
$CPE_2$	0.9028
$R_2$ (Ohm·cm <sup>2</sup> )	3827

The result of the model proposed is the equivalent circuit depicted in Figure 10 and this may be used to evaluate the Ti–Zr alloy/electrolyte interface. It consists of  $R_s$ , the electrolyte resistance,  $CPE_{dl}$  and the pseudo-capacitance.  $R_{ct}$  is the oxide film resistance,  $CPE_2$  is the pseudo-capacitance of the double layer, and  $R_2$  is the charge transfer resistance at the electrode/solution interface. As one may see from Table 3, the electrolyte resistance value is in the range of 1–2 Ohm·cm<sup>2</sup> which indicates a typical value for the given oxide mixture, while  $CPE_{dl}$  is in the range of 0.5–1 F·cm<sup>-2</sup> which indicates the presence of cracks and some other defects in the mixed-oxide layer structure; this fact is confirmed by SEM analysis.

The composition of the sample surfaces is also influenced by the applied surface functionalization treatments. The evolution of the composition of the investigated surfaces

according to the functionalization method applied is presented in Figure 9. As a general observation, on all the analyzed samples, we reported the presence of contamination with C between 6 and 11%at, but also with Hf < 0.25%at. The contamination with C can be explained by its presence in the anodization electrolyte of the oxalic acid (has the role of promoting the formation of mixed-oxide nanotubes), and its concentration decreases almost by half after the thermal treatment (~6%at P2), when part of this C is converted into carbon dioxide and purged by the forced air flow.

Small concentrations of hafnium may appear because this element usually accompanies titanium and zirconium, and the manufacturer of the alloy did not consider it necessary to report it at such low concentrations. We can also observe a significant increase in the concentration of O, up to 10× even, as a result of the applied treatments which are explained, taking into considerations that the anodization process promotes the formation in situ of oxygen, and the thermal treatment takes place in connection with an additional intake of air, and implicitly oxygen. In the case of the anodized samples, DAT3 and DAT4 samples, the presence of F contamination was observed, and these traces are the result of the functionalization by anodization; the electrolyte used in the anodization contained ammonium fluoride, with its concentration decreasing to less than 0.5%at in sample DAT4 due to the post-anodization thermal treatment, and hence another inherent benefit of the post-anodization thermal treatment, that of additional cleaning. A possible strategy to entirely remove fluoride from the anodization electrolyte involves increasing the concentration of ionic liquids to offset this removal. However, this adjustment must be executed with caution to prevent adversely affecting the formation of the nano-structured oxide on the alloy surface, as fluoride ions appear to play a crucial role in this process.

The concentrations of titanium and zirconium decrease for sample DAT2, with respect to that of oxygen, as a result of the thermal treatment at 450 °C in air, confirming the observation that even by thermal treatment alone, the mixed-oxide layer increases in size and mass. The experimental data obtained for Shore HD hardness and presented in Table 2 were converted by means of a transfer function (presented in detail in the Supplementary Materials) and the comparative results of the mixed-oxide hardness expressed as Shore D and Brinell values are shown in Table 4 below.

**Table 4.** The mixed-oxide hardness expressed as Shore D and Brinell values of the analyzed samples.

	D <sub>Shore HD</sub>	D <sub>Brinell</sub>
Anodization	2.7	22.59
Anodization and thermal treatment	16.5	27.20

As one may see from Table 4, the thermal treatment applied after anodization leads to an increase in hardness of about 6.1 folds (610%) enhancing the mechanical properties, namely the oxide layer hardness. This is probably due to the conversion of the amorphous form of titanium and zirconium mixed oxides obtained by anodization into the crystalline form of rutile, a transformation substantiated theoretically and practically in the scientific literature [11]. The increase in hardness is beneficial for enhancing the oxide layer mechanical properties, it allows an easy polish of the final product, and it promotes better cell adhesion.

#### 4. Conclusions

The measurements of the OCP variation over time showed that the analyzed Ti–Zr alloy has the necessary susceptibility to be subjected to the anodization process in order to electrochemically form a stable oxide layer on the surface of this alloy. The model obtained from the electrochemical impedance spectroscopy data can be useful in quantitative evaluations, as the value of the resistance  $R_{ct}$  can be easily deduced; this is directly correlated with the thickness of the oxide layer formed and, in this way, we have a referential system of comparison for the oxide layers formed. The thermal treatment has a



beneficial effect from the point of view of surface decontamination, eliminating much of the organic carbon contamination, as well as the ammonium fluoride, the latter dropping from ~8%at to < 0.5%at for samples subjected to post-anodization thermal treatment. The anodized samples have a morphology characterized by a micro-nano-porous surface, which can be of favorable support in restorative dentistry for the anchoring of osteoblast or mesenchymal cells onto the mixed-oxide layer. The anodization in ionic liquids (electrolytes containing e.g., choline chloride) can be successfully conducted at constant current values, but also at reduced values of applied voltage comparing to that carried out in fluorinated electrolytes in the absence of ionic liquids. This may lead to a decreased number of defects in the resulting oxide layer, so anodizing in ionic liquid seems to be a promising technique for obtaining better mixed-oxide layers. The applied thermal treatment is a beneficial one, allowing an increase of six folds in the value of hardness for thermally treated samples.

**Supplementary Materials:** The following supporting information can be downloaded at: <https://www.mdpi.com/article/10.3390/coatings14091217/s1>, Figure S1: Materials for polishing Ti/Zr alloy disks; Figure S2: Working electrode. T-Zr alloy disk held in place by a Ti rod provided with a slit at the lower end; Figure S3: Experimental protocol and operating parameters for OCP; Figure S4: Experimental protocol and operating parameters for EIS; Figure S5: Experimental protocol and operating parameters for OCP; Figure S6: Experimental protocol and operating parameters for EIS; Figure S7: Equivalence between Shore D and Rockwell R hardness classes; Figure S8: Comparison chart between different hardness scales (Brinell, Rockwell B, Rockwell C, Shore); Figure S9: Digital Hardness tester Shore D. Figure S10: Rockwell hardness as a function of Shore D hardness; Figure S11. Rockwell hardness as a function of Shore D hardness; Figure S12: SEM-EDXS on three distinct aria for DAT1: Aria 1; Aria2; Aria3; Figure S13: SEM-EDXS on three distinct aria for DAT2: Aria 1; Aria2; Aria3; Figure S14: SEM-EDXS on three distinct aria for DAT3: Aria 1; Aria2; Aria3; Figure S15: SEM-EDXS on three distinct aria for DAT4: Aria 1; Aria2; Aria3; Table S1: Air blower pump calibration data; Table S2: Oven calibration data; Table S3: Shore D hardness tester calibration according to the sensor profile; Table S4: SEM-EDXS on three distinct zones/aria for DAT1; Table S5: SEM-EDXS on three distinct zones/aria for DAT2; Table S6: SEM-EDXS on three distinct zones/aria for DAT3; Table S7: SEM-EDXS on three distinct zones/aria for DAT4.

**Author Contributions:** Conceptualization, D.-I.V., I.-A.C. and A.C.; methodology, A.C., I.-A.C. and D.-I.V.; validation, A.C., I.-A.C., D.-I.V., R.B. and F.B.I.; investigation, A.C., I.-A.C. and D.-I.V.; data curation I.-A.C. and A.C.; writing—original draft preparation, D.-I.V., figure A.C. and I.-A.C.; writing—review and editing, I.-A.C., A.C. and D.-I.V.; visualization, D.-I.V., I.-A.C., F.B.I., A.C. and R.B.; project administration, D.-I.V. and R.B.; funding acquisition, R.B. All authors have read and agreed to the published version of the manuscript.

**Funding:** This research was supported by Dentix Millennium SRL through the project “Functionalization of the transmucosal surface of prosthetic abutments on dental implants for peri-implant space sealing”, code MySMIS 122040, contract no. 361/390037/27.09.2021 concluded with Romanian Research, Innovation and Digitalization Minister, Research Intermediary Body General Direction.

**Data Availability Statement:** Data are contained within the article and Supplementary Materials.

**Acknowledgments:** Roxana Budei registered with the University of Medicine and Pharmacy “Carol Davila” Bucharest. Special thanks go to Corneliu Andrei from the National University of Science and Technology Politehnica Bucharest, Faculty of Chemical Engineering and Biotechnology for providing the necessary logistic support for this work.

**Conflicts of Interest:** Author Roxana Budei was employed by the company Dentix Millennium SRL. The remaining authors declare that the research was conducted in the absence of any commercial or financial relationships that could be construed as a potential conflict of interest.

## References

1. Zhao, Q.; Ueno, T.; Wakabayashi, N. A review in titanium-zirconium binary alloy for use in dental implants: Is there an ideal Ti-Zr composing ratio? *Jpn. Dent. Sci. Rev.* **2023**, *59*, 28–37. [[CrossRef](#)] [[PubMed](#)]
2. Li, G.; Shen, E.; Liang, L.; Li, K.; Lu, Y.; Zhu, W.; Tian, Y.; Baker, I.; Wu, H. Microstructure and corrosion resistance of powder metallurgical Ti-Nb-Zr-Mg alloys with low modulus for biomedical application. *Mater. Charact.* **2022**, *192*, 112223. [[CrossRef](#)]



3. Cordeiro, J.M.; Faverani, L.P.; Grandini, C.R.; Rangel, E.C.; da Cruz, N.C.; Nociti, F.H., Jr.; Almeida, A.B.; Vicente, F.B.; Morais, B.R.G.; Barão, V.A.R.; et al. Characterization of chemically treated Ti-Zr system alloys for dental implant application. *Mater. Sci. Eng. C* **2018**, *92*, 849–861. [[CrossRef](#)]
4. Kozak, M.; Mazierski, P.; Baluk, M.; Żebrowska, J.; Lisowski, W.; Trykowski, G.; Skowron, P.; Zaleska-Medynska, A. Anodized multi-component titanium alloys carrying antibacterial features. *Appl. Surf. Sci.* **2023**, *613*, 156009. [[CrossRef](#)]
5. Tang, K.; Luo, M.L.; Zhou, W.; Niu, L.N.; Chen, J.H.; Wang, F. The integration of peri-implant soft tissues around zirconia abutments: Challenges and strategies. *Bioact. Mater.* **2023**, *27*, 348–361. [[CrossRef](#)] [[PubMed](#)]
6. Liu, J.; Pathak, J.L.; Hu, X.; Jin, Y.; Wu, Z.; Al-Baadani, M.A.; Wu, S.; Zhang, H.; Farkasdi, S.; Liu, Y.; et al. Sustained release of zoledronic acid from mesoporous TiO<sub>2</sub>-layered implant enhances implant osseointegration in osteoporotic condition. *J. Biomed. Nanotechnol.* **2018**, *14*, 1965–1978. [[CrossRef](#)] [[PubMed](#)]
7. Dong, H.; Liu, H.; Zhou, N.; Li, Q.; Yang, G.; Chen, L.; Mou, Y. Surface modified techniques and emerging functional coating of dental implants. *Coatings* **2020**, *10*, 1012. [[CrossRef](#)]
8. Farrag, K.M.; Khamis, M.M. Effect of anodized titanium abutment collars on peri-implant soft tissue: A split-mouth clinical study. *J. Prosthet. Dent.* **2021**, *130*, 59–67. [[CrossRef](#)]
9. Makurat-Kasprolewicz, B.; Ossowska, A. Recent advances in electrochemically surface treated titanium and its alloys for biomedical applications: A review of anodic and plasma electrolytic oxidation methods. *Mater. Today Commun.* **2023**, *34*, 105425. [[CrossRef](#)]
10. Gulati, K.; Martinez, R.D.O.; Czerwiński, M.; Michalska-Domańska, M. Understanding the influence of electrolyte aging in electrochemical anodization of titanium. *Adv. Colloid. Interface Sci.* **2022**, *302*, 102615. [[CrossRef](#)]
11. Pauporté, T.; Finne, J.; Lincot, D. Impedance spectroscopy study of anodic growth of zirconium oxide film in NaOH medium. *Phys. Stat. Sol.* **2005**, *202*, 1502–1507. [[CrossRef](#)]
12. Wu, S.; Luo, X.; Long, Y.; Xu, B. Exploring the phase transformation mechanism of titanium dioxide by high temperature in situ method. In Proceedings of the 2nd International Conference on Frontiers of Materials Synthesis and Processing, IOP Conference Series Proceedings: Materials Science and Engineering, Sanya, China, 10–11 November 2018; p. 012010.
13. Körkel, A.F.K.; Jellesen, M.S.; Foss, M.; Ceccato, M.; Somers, M.A.J.; Christiansen, T.L. Thermochemical oxidation of commercially pure titanium; controlled formation of robust white titanium oxide layers for biomedical applications. *Surf. Coat. Technol.* **2023**, *467*, 129716. [[CrossRef](#)]
14. Kumar, A.; Barbhuiya, N.H.; Singh, S.P. Magnéli phase titanium sub-oxides synthesis, fabrication and its application for environmental remediation: Current status and prospect. *Chemosphere* **2022**, *307*, 135878. [[CrossRef](#)] [[PubMed](#)]
15. Liu, J.; Hong, G.; Wu, Y.H.; Endo, K.; Han, J.M.; Kumamoto, H.; Wada, T.; Kato, H.; Gao, P.; Sasaki, K. A novel method of surface modification by electrochemical deoxidation: Effect on surface characteristics and initial bioactivity of zirconia. *J. Biomed. Mater. Res. Part B Appl. Biomater.* **2017**, *105*, 2641–2652. [[CrossRef](#)] [[PubMed](#)]
16. Roy, P.; Berger, S.; Schmuki, P. TiO<sub>2</sub> nanotubes: Synthesis and applications. *Angewandte Chemie Int. Ed.* **2011**, *50*, 2904–2939. [[CrossRef](#)] [[PubMed](#)]
17. Losic, D.; Simovic, S. Self-ordered nanopore nanotube platforms for drug delivery applications. *Expert Opin. Drug Deliv.* **2009**, *6*, 1363–1381. [[CrossRef](#)]
18. Tsuchiya, H.; Macak, J.M.; Taveira, L.; Schmuki, P. Fabrication characterization of smooth high aspect ratio zirconia nanotubes. *Chem. Phys. Lett.* **2005**, *410*, 188–191. [[CrossRef](#)]
19. Guo, L.; Zhao, J.; Wang, X.; Xu, R.; Lu, Z.; Li, Y. Bioactivity of zirconia nanotube arrays fabricated by electrochemical anodization. *Mater. Sci. Eng. C* **2009**, *29*, 1174–1177. [[CrossRef](#)]
20. Jennes, M.E.; Naumann, M.; Peroz, S.; Beuer, F.; Schmidt, F. Antibacterial effects of modified implant abutment surfaces for the prevention of peri-implantitis—A systematic review. *Antibiotics* **2021**, *10*, 1350. [[CrossRef](#)]
21. Li, X.; Li, C.; Gong, T.; Su, J.; Zhang, W.; Song, Y.; Zhu, X. Comparative study on the anodizing process of Ti and Zr and oxide morphology. *Ceramics Int.* **2021**, *47*, 23332–23337. [[CrossRef](#)]
22. Chen, S.; Ni, Y.; Zhang, J.; Dan, Y.; Zhang, W.; Song, Y.; Chen, X. Double-anode anodization of metal Ti in two beakers. *Electrochem. Comm.* **2021**, *125*, 106991. [[CrossRef](#)]
23. Guo, T.; Ivanovski, S.; Gulati, K. Optimizing titanium implant nano-engineering via anodization. *Mater. Des.* **2022**, *223*, 111110. [[CrossRef](#)]
24. Bordbar-Khiabani, A.; Gasik, M. Electrochemical and biological characterization of Ti–Nb–Zr–Si alloy for orthopedic applications. *Sci. Rep.* **2023**, *13*, 2312. [[CrossRef](#)] [[PubMed](#)]
25. Strnad, G.; Jakab-Farkas, L.; Gobber, F.S.; Peter, I. Synthesis and Characterization of Nanostructured Oxide Layers on Ti–Nb–Zr–Ta and Ti–Nb–Zr–Fe Biomedical Alloys. *J. Funct. Biomater.* **2023**, *14*, 180. [[CrossRef](#)]
26. ISO 868:2003; Plastics and Ebonite—Determination of Indentation Hardness by Means of a Durometer (Shore Hardness). ISO: Geneva, Switzerland, 2003.

**Disclaimer/Publisher’s Note:** The statements, opinions and data contained in all publications are solely those of the individual author(s) and contributor(s) and not of MDPI and/or the editor(s). MDPI and/or the editor(s) disclaim responsibility for any injury to people or property resulting from any ideas, methods, instructions or products referred to in the content.